A Model for Studying the Biomechanical Effects of Varying Ratios of Collagen types I and III on Cardiomyocytes

Brian Roman[1,1a], Shweta Anil Kumar[1,1a], Shane C. Allen[2], Monica Delgado[1,1a], Sabastian Moncayo[1a], Andres M. Reyes[3], Laura J. Suggs[2], Ramana Chintalapalle[4], Chunqiang Li[3,5], Binata Joddar[1,5]*

[1] Inspired Materials & Stem-Cell Based Tissue Engineering Laboratory (IMSTEL),

[1a] Department of Metallurgical, Materials and Biomedical Engineering, University of Texas at El Paso, 500 W University Avenue, El Paso, TX 79968, USA.

[2] Department of Biomedical Engineering, The University of Texas at Austin, Austin, Texas 78712, USA.

[3] Department of Physics, The University of Texas at El Paso, 500 W University Avenue, El Paso, Texas 79968, USA.

[4] Department of Mechanical Engineering, The University of Texas at El Paso, 500 W University Avenue, El Paso, Texas 79968, USA.

[5] Border Biomedical Research Center, University of Texas at El Paso, 500 W University Avenue, El Paso, TX 79968, USA.

* Correspondence: Binata Joddar; bjoddar@utep.edu; Phone: (915) 747-8456, Fax: (915) 747-8036.

Abstract:

Collagen I (Col I) and III (Col III) present in the cardiac tissue are homeostatically maintained in the ratio of 3:1 to promote cardiac health. Increase in the relative amounts of Col I leads to an imbalance of Col I:III during cardiac-fibrosis, which has damaging effects on cardiac myocytes (CM). Substrate gels composed of Col I:III ratios of 9:1 and 3:1, were developed to represent fibrous- and normal-cardiac tissue, and used to study resultant changes in CM function. Second harmonic generation microscopy used to image Col I, displayed a decrease in acquired image intensity with an increase in the non-second harmonic Col III in 3:1 gels. SEM showed a fiber-rich structure in the 3:1 gels with well-distributed pores unlike the 9:1 gels or the 1:0 controls. Rheological analysis showed a decrease in substrate stiffness with an increase of Col III, in comparison with other cases. CM cultured within 3:1 gels exhibited an elongated rod-like morphology with an average end-to-end length of 86 ± 28.8 μm characteristic of healthy CM, accompanied by higher cell growth in comparison with other cases. Finite element analysis used to estimate the forces exerted on CM cultured in the 3:1 gels, showed that the forces were well dispersed, and not concentrated within the center of cells, in comparison with other cases. This study model can be adopted to simulate various biomechanical environments in which cells crosstalk with the Col-matrix in diseased pathologies to generate insights on strategies for prevention of fibrosis.

Keywords

Collagen type-I, Collagen type-III, Cardiomyocytes, Cardiac Fibrosis, Cell Morphology, Tensile Stress

1. Introduction

Collagen has long been a biomaterial of interest in tissue engineering, as it is found within the extracellular matrix (ECM) in high amounts and its biocompatibility makes it well accepted by cells (Carrow et al. 2015; Glowacki and Mizuno 2008). Being a structural protein found within the ECM of connective tissue, multiple types exist with the most common being types I, II, III, IV, and V, allowing for distinct functions within each tissue. Type II collagen is attributed to being the main component of hyaline cartilage, however it is also the component of structures found within the eye. Types I, III, and V on the other hand, form macrostructures capable of providing tensile strength to areas of great stress such as that of bone, ligaments, and tendons.

In this study, we focus on Collagen types I and III and their role in the heart, where their fibrous nature provides the backbone for cardiac tissue, acting as a scaffold for CM. Col I and Col III both reside in the heart, with Col I being the more abundant of the two. A healthy myocardial ECM is comprised of 2-4% collagen (Talman and Ruskoaho 2016). Of this percentage, the typical cardiac muscle contains a 3:1 ratio of Col I and Col III (Jugdutt 2003), whereas a fibrotic cardiac muscle contains a ratio of 9:1 of Col I and III (Pauschinger et al. 1998). The upregulation of Col I is often seen after myocardial infarction (MI) and is thought to be the cause of the stiffening of cardiac tissue by disrupting the normal ratio of 3:1 ratio of Col I and Col III (Brower et al. 2006; Yu et al. 2018; Pathak et al. 2001). During such an event, CMs in the left ventricle undergo a state of necrosis and cardiac fibroblasts (CF) are seen to be replaced by myofibroblasts (MF) (Fan et al. 2012). These MF are known to be the cause behind the significantly higher Col I concentrations leading to cardiac fibrosis, a scarring process that impacts cardiac structure and function overtime leading to heart failure (Weber and Díez 2016; Richardson et al. 2015; Chistiakov, Orekhov, and Bobryshev 2016). Thus, therapy directed at cardiac fibrosis could reduce the progression of heart failure and other related cardiac disorders.

Collagen gels are commonly used as 3D scaffolds that provide a similar environment to that found in the wound healing process of connective tissue (Frahs et al. 2018). Previous studies have focused on the effects of Col I on CF, CM and MF; however, the addition of Col III provides an ECM environment more characteristic of in vivo cardiac tissue.

This study introduces a new model solely composed of Col I and Col III in which the structural and mechanical behavior of resident CM can be studied. Lower and upper limits were set to include the ratios of Col I and Col III in 3:1 and 9:1, as the progression of fibrosis due to change in ratios of Col I:III was tested. Previous studies that have attempted to fabricate such Collagen-rich models have included the use of additional ingredients such as that of chondroitin sulfate and potassium chloride whereas the model developed by us consists of Col I and III only to mimic ratios found in healthy and diseased heart wall (Stuart and Panitch 2009). Specific advantages conferred by the Col I and III model in this study include the ability to depict interactions among cells and ECM that may explain the progression of MI in cardiac tissue and lead to the development of clinical phenotypes. The resultant effects of different Col I:III ratios on CM can be compared by studying the cell behavior of CM in each gel of varying Col I and III concentrations. As stiffness of the ECM is known to govern cellular behavior, mimicking physiological changes that occur as a result of an imbalance in Col I and III leading to alteration of the ECM is an essential step in strategizing approaches for restoring CM function in the cardiac tissue (Asgari et al. 2017). In this study, variation in resultant gel structures due to inclusion of variable ratios of Col I:III was confirmed using scanning electron microscopy (SEM). Their viscoelastic properties were studied using rheological analysis and their differing composition was confirmed by second-harmonic generation (SHG) imaging and microscopy. Following the characterization of gels, their biocompatibility and effects on cellular morphology and function was studied with respect to the varying ratios of Col I:III in each gel on CM using phase contrast microscopy and a cell trace violet (CTV) proliferation assay. Finite element analysis (FEA) was used to obtain a simulated estimation of the force experienced by cells in the collagen gels with varying ratios of Col I:III.

2. Methods

2.1 Materials, Reagents and Kits

A 3D Collagen Culture Kit containing Collagen I solution, Medium 199, and Neutralization solution for the formation of collagen gels, was used following the manufacturers recommendations (Cat. No. ECM765,

MilliporeSigma, Burlington, MA). Purified Collagen Type III (Bovine, Cat. No. CC078) were obtained from ThermoFisher Scientific (Waltham, MA). For cell culture in the collagen gels, 1% Penicillin-Streptomycin and EmbryoMax L-Glutamine Solution (100X) were obtained from Millipore. Fetal Bovine Serum was obtained from Gibco (ThermoFisher Scientific). Dulbecco's Modified Eagle's Medium/Nutrient Mixture F-12 Ham with 15mM HEPES and sodium bicarbonate was obtained from ATCC (Manassas, VA), and 0.25% trypsin-EDTA was obtained from ThermoFisher Scientific. Cell Trace Violet (CTV), proliferation kit was obtained from Invitrogen (Carlsbad, CA). 4% paraformaldehyde was obtained from Sigma-Aldrich (St. Louis, MO).

2.2 Preparation of Collagen gels

As 3D scaffolds have become predominantly used to explore the effects of materials on different cellular functions, we fabricated gels composed of varying Col I:III ratios. These include a 3:1 ratio similar to that found in healthy cardiac tissue and a 9:1 ratio representative of tissue afflicted with cardiac disease. A gel made of 100% Col I (Col I: III = 1:0) was also fabricated as a control for all in vitro experimental analysis (Joddar et al. 2016). The control gels made from Col I only, involved an acidic Col I solution to which the neutralization solution consisting of sodium hydroxide was added to cause a polymerization to the matrix within 15 - 30 minutes and lead to formation of gels (Z. Chen et al. 2011).

The Col I solution was formed by mixing bovine collagen I solution, 5X M199 medium with phenol red, FBS, and adjusting the pH with neutralization solution. The percentages for each constituent were as follows: 70.2% bovine collagen III solution, 17.6% 5X M199 medium with phenol red, 10% FBS, and 2% neutralization solution (Table 1). Col III solution was formed by the addition of 0.8µL of 0.5M acetic acid for each µg of bovine collagen III powder and stirring it overnight at 4°C. Acetic acid was then added until the solution reached a 1µg/µL concentration and 0.5M of sodium hydroxide is added accordingly, neutralizing the pH. The observed gel ratios were obtained by combining the appropriate amounts of each collagen solution into a homogeneous mixture followed by incubation at 37°C for an hour or until gelation was observed. All gels were prepared in the

same manner with the only difference being the change in ratio when adding the respective amounts of Col I and III (Table 1). It is to be noted that Col III does not form stable gels by itself under the same protocol used for Col I as Col III is studied more extensively for its effects alongside Col I rather than by itself (Nielsen and Karsdal 2016). Therefore, it was incorporated into existing Col I gels in varying proportions, as described in Table 1.

Table 1. The constitution for making solutions of Collagen I and III is depicted in **(a)** and **(b)** respectively. The scheme for forming gels is outlined in **(c)** for formation of gels with 100% Collagen I, and Collagen I:III gelled together in ratios of 9:1 and 3:1 respectively. For these gels, the Collagen III solution was immediately added to Collagen I solution with gels allowed to form by incubation for 1 hr. at 37°C along with addition of neutralization solution added to solution of Collagen I.

(a) Preparation of Collagen I Solution

Collagen I (µL)	Medium 199 (µL)	FBS (µL)
1200	300	170.1

(b) Preparation of Collagen III Solution

Collagen III Powder (µg)	0.5M Acetic Acid (µL)	0.5M NaOH (µL)
360	360	373

(c) Preparation of Collagen I/III Solutions

Ratio of Collagen I: Collagen III	Collagen I Solution (µL)	Collagen III Solution (µL)
1:0 (100% Collagen I)	200	0
9:1	180	20
3:1	150	50

2.3 Absorbance Assay

Gelation of 9:1 and 3:1 collagen solutions was confirmed through an absorbance assay being observed over time with a Molecular Devices VersaMax UV/Vis Plate Reader equipped with a VersaMax SoftMax® Pro Software (Molecular Devices, LLC. San Jose, CA). An absorbance assay was also performed on the 1:0 sample to acquire absorbance measurements confirming gelation in these standard or control samples. Transmittance of light through each collagen solution was measured over a period of 300 seconds at a wavelength of 562 nm (Blissett et al. 2009). Col I and III solutions were prepared (Table 1) and placed inside a 96-well plate with n=3. Mathematica 11ª was used to analyze the data and obtain transmittance curves for each of the 9:1 and 3:1 gel ratios.

2.4 Rheological analysis

Rheometric analysis was performed on the each of the collagen gels prepared as described earlier to determine the varying stiffness's and rheological parameters in gels made with varying ratios of Col I:III (AnilKumar et al. 2019). A biopsy punch was used to cut out gel discs with dimensions of 8 mm diameter and 1 mm thickness. Prior to the test, these gel discs were immersed in 1X PBS and allowed to swell to equilibrium. An Anton-Paar MCR101 rheometer (Anton-Paar, Graz, Austria) with an 8-mm parallel plate geometry, was used to perform oscillatory shear stress rheometry at 1% strain and a frequency of 0.5-50 Hz. Frequency sweeps were done to determine the strain and frequency range within the viscoelastic range of the gels. The complex viscosity was measured at 1.99 Hz and the elastic and complex shear moduli were calculated using the generated values of storage and loss moduli, as was done earlier (Anil Kumar et al. 2019).

2.5 Second Harmonic Generation (SHG)

3-Dimensional characterization of collagen samples were observed using a home-built SHG microscope (Acosta et al. 2014). The light source is a mode-locked femtosecond Ti:Sapphire laser (Maitai HP, wavelength 690-1040 nm, 100 fs, 80 MHz, Newport, Santa Clara, California). The wavelength was set at 930 nm to generate

SHG signal at 465 nm. The blue detection channel has a bandpass filter (417-477 nm) to selectively detect this SHG signal. The laser power at the sample site was set at 20 mW with a half waveplate and a polarizing beam splitter. Solutions intended for forming gels of each Col I:III ratio were mixed (Table 1) and pipetted directly on glass slides, 75mm x 25mm. Next, this 100 µl pipetted solution placed onto the glass slides, was mounted with thin cover glasses (25mm x 25mm) and the samples placed in an incubator (37°C, 1 h) to promote gelation of all samples. This technique allowed preparation of samples having an approximate thickness of ~100µm. Once gelation was confirmed by the visual detection of collagen fibrils in each sample using a bright field EVOS XL Core (ThermoFisher Scientific) microscope, they were subjected to SHG microscopy and images were acquired with a wavelength of 930nm being used to generate second harmonic oscillations within each collagen sample. All images were acquired with the same excitation power, and the intensities were directly comparable. Controls included 5X M199 medium with phenol red pipetted onto glass slides and imaged. Acquired images were processed using ImageJ (NIH) to convert the raw images (blue) into thresholded images (B&W) for calculation of collagen fiber lengths (X. Chen et al. 2012).

2.6 Scanning Electron Microscopy (SEM)

Scanning Electron microscopy (SEM) was used for acquiring cross sectional images of lyophilized collagen gels in accordance with published works (Anil Kumar et al. 2018). Uniform sized gels were prepared, lyophilized, sputter coated (Gatan Model 682 Precision Etching Coating System, Pleasantown, CA, USA) and imaged under an accelerating voltage of 13 kV, using SEM (S-4800, Hitachi, Japan). Acquired images were further analyzed using ImageJ to estimate the average pore diameter for each sample analyzed.

2.7 Cell culture in Collagen gels

AC16 Human CM cell lines (Millipore Sigma) were cultured in complete Growth Medium and passaged for in vitro stabilization prior to being used in experiments. The complete Growth Medium consisted of Dulbecco`s Modified Eagle`s Medium/Nutrient Mixture F-12 with 15mM HEPES and sodium bicarbonate, liquid

sterile-filtered, suitable for cell culture. To this, we added 12.5% Fetal Bovine Serum, 1% Penicillin-Streptomycin and 200mM L-Glutamine. The cells were cultured, passaged and stabilized for at least six passages before being used in experiments with medium being changed every 24 hr. At the end of every passage, normal and healthy cell morphology was confirmed using phase contrast image acquired using EVOS Imaging Systems displaying the morphology of healthy CM. These were then seeded atop each collagen sample post-gelation at a density of 4 X 10^5 cells/mL within 48-well plates and were incubated for 72 hr (37°C, 5% CO_2), after which were fixed using 100 µL of 4% paraformaldehyde (Sigma-Aldrich) in each well for 20 minutes. The samples were then washed with 1X Phosphate Buffered Saline (PBS) and analyzed using phase-contrast microscopy (ZEISS Axio Observer. A1 LSM 700, Germany) to elucidate the effects of varying Col I:III concentrations on CM. Images of cells in gels were acquired after 48 hr when the cells were accustomed to their respective collagen substrates.

The effects of varying Col I and III concentrations on CM morphology while knowing the Young's modulus of the substrate gels can be used to predict the forces applied by the substrate on the CM (del Álamo 2007). For this purpose, average cell diameter and end-to-end length were acquired for cells cultured in each Col I:III ratio to elucidate the effect an increase in Col I, compared with Col III, has on CM morphology. The extension of CM to a rod-like shape, is imperative for sarcomere contraction (Ribeiro et al. 2015). Additionally, retention of optimal cell diameter is attributed to the cell surface area: volume ratio, which may limit a cell's ability to diffuse nutrients if the CM becomes too enlarged (Chang and Huang 2014). Thus, end-to-end length and diameter of cells were hence obtained through the use of ImageJ by following previous work, allowing for a comparison between CM parameters on varying Col I:III ratios (Anil Kumar et al. 2019). The cellular aspect ratio was then obtained by dividing the average end-to-end length over the average cell diameter of each respective ratio (Col I:III), as shown by the formula:

$$\text{Cellular Aspect Ratio (unit less)} = \frac{\text{Average Cell End-to-End Length}}{\text{Average Cell Diameter}} \qquad (1)$$

2.8 Cell Trace Violet (CTV) Assay

To estimate their proliferation in the collagen gels, encapsulated cells were pre-stained using CTV proliferation kit (Invitrogen, Carlsbad, CA, USA) and subjected to Flow Cytometry (FACS) analysis, as done earlier (Anil Kumar et. al 2019) following manufacturer's protocols. The CTV dye was applied at 1:1000 dilution in this study, for pre-staining cells. These pre-stained cells were mixed with the solutions placed within 96 wells, cross-linked for gelation and cultured for 24 hr, and 72 hr respectively (37°C, 5% CO_2). After 24- and 72-hr, cell-gel samples were treated using Trypsin-EDTA (0.25%, phenol red) (ThermoFisher), after which the detached cells were carefully extracted and processed for flow cytometry (FACS). Extracted cells were fixed and processed further for FACS (Beckman Coulter Gallios Flow Cytometer, Brea, CA, USA) using excitation and emission wavelengths of 405 and 450 nm respectively. Positive controls included pre-stained cells grown on plastic petri dishes for 24 and 72 hrs, respectively. Negative controls included non-stained cells grown on plastic petri dishes for 24 and 72 hrs, respectively. Results were presented as the % of cells expressing the CTV dye after each characteristic sample run at 24 and 72 hrs, respectively. In addition, the extent of cell proliferation for each case was calculated using formula (2) below:

$$\text{Extent of Proliferation} = \frac{\%\ \text{Cells Expressing CTV after 24 hr-}\%\ \text{Cells Expressing CTV after 72 hr}}{\%\ \text{Cells Expressing CTV after 24 hr in 1:0 sample}} \times 100 \quad (2)$$

2.9 Cell Morphology Analysis and Force Estimation

To simulate the applied force on each cell, Finite Element Analysis (FEA) was performed on CM from each sample using Fusion 360 (Autodesk, Inc. San Rafael, CA). CM thickness was estimated to be 20 μm by using the average CM thickness shown in a cross-sectional profile of the left and right ventricles in vivo (Tracy 2014). A force of 1.12×10^{-6} N was obtained by multiplying the known diastolic stress applied in vivo, by the average area of a CM and was subsequently applied to each cell (Frisk et al. 2016). In order to accurately model the behavior

experienced by CM in their natural environment, the edges and bottom surface of all cells were locked in the x, y, and z direction, with the load being applied on the top surface. FEA was done on a static stress environment, with testing conditions being identical throughout each Col I:III ratio.

2.10 Statistical Analysis

All samples were present in groups of three and all experiments were performed twice, unless otherwise mentioned. Data are represented as the Mean ± Standard Deviation. Microsoft Excel Student's *t*-test was performed to determine if the averages of any two of the sample datasets compared showed significant difference in their values. p-values less than 0.05 were considered statistically significant.

3. Results

3.1 Absorbance Assay

Gel formation of 3:1 and 9:1 collagen solutions was confirmed and quantified through absorbance assays (Fig. 1a, b). Both collagen ratios attained a transmittance of 40% after 300 s. These results confirmed gelation for both sets of gels containing 3:1 and 9:1 collagen solutions, in comparison with controls (Supplementary Fig. 1). Supplementary Fig. 1 depicts characteristic absorbance of all gels pre-and post-gelation confirming gelation of all samples. Although not depicted, we attempted to form Col I:III gels composed of 1:1 and 0:1 ratios. These however, did not undergo crosslinking and remained a solution after 300 s.

3.2 Rheological Parameters

Gel discs formed from all groups exhibited clear elastic behavior (Figure 2a, b, c). The equilibrium of both storage and loss modulus was found between frequencies ranging from 0.5Hz to 50Hz, which corresponded to a linear viscoelastic region. Utilizing these behaviors, the storage and loss modulus were determined for gels of varying Col I:III ratios. Decreasing Col I fraction decreased both storage and loss modulus, indicating higher elasticity in gels with greater concentration of Col I (Figure 2d). Interestingly, decreasing Col I concentration

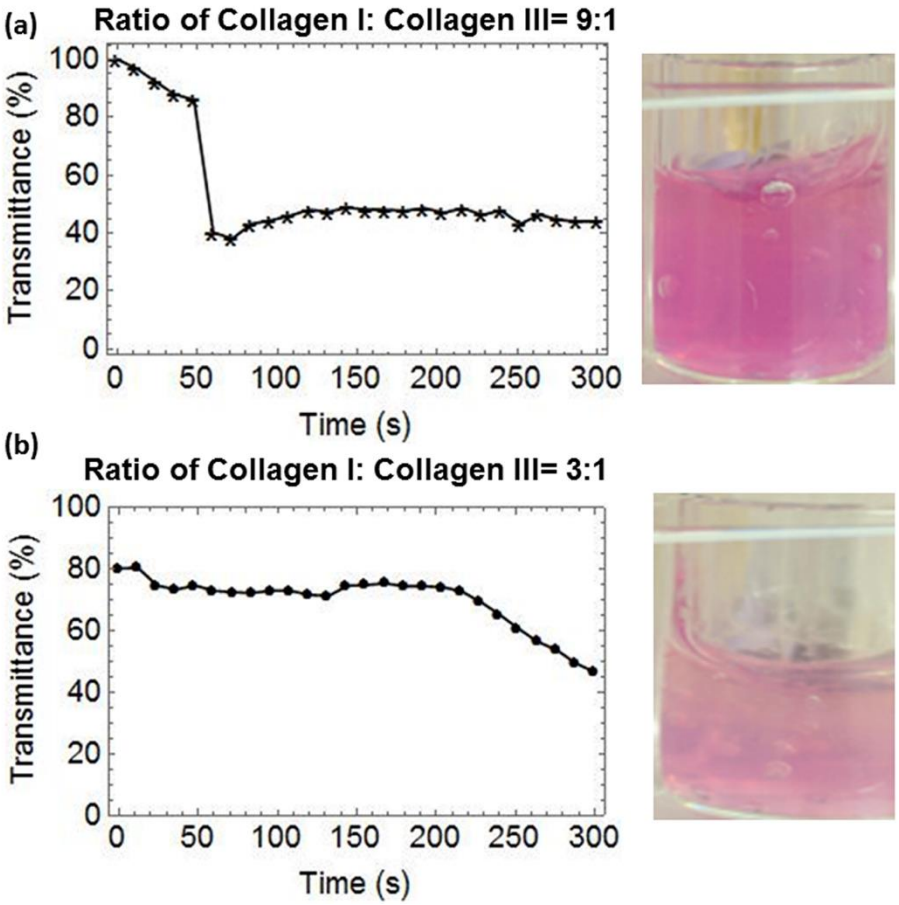

Fig. 1: Absorbance assay to confirm gelation for Collagen I:III mixtures. Shown are transmittance curves (left) depicting the rate of gelation, and corresponding images of formed gels in wells (right) confirming the solutions have undergone gelation, for (**a)** 9:1 ratio (∗) and (**b)** 3:1 ratio (•) of Collagen I:III respectively.

further decreased the complex viscosity, implying changes to the microstructure (Figure 2e) (Shayegan and Forde 2013).

From the rheological data, a semi-logarithmic function was established to estimate the amount of Col I and concurrently of Col III, based on the corresponding Young's modulus of the collagen gel sample. The natural log of the average Young's modulus for each ratio was taken and attributed to the amount of Col I present within the gel as displayed by Supplementary Figure 2a. Average values of the viscoelastic properties of each collagen gel showed a decrease as the concentration of Col I was reduced (Supplementary Figure 2b). This can be attributed to Col I fibers being thicker than those of Col III, as they provide great structural strength within the cardiac ECM (Jugdutt 2003).

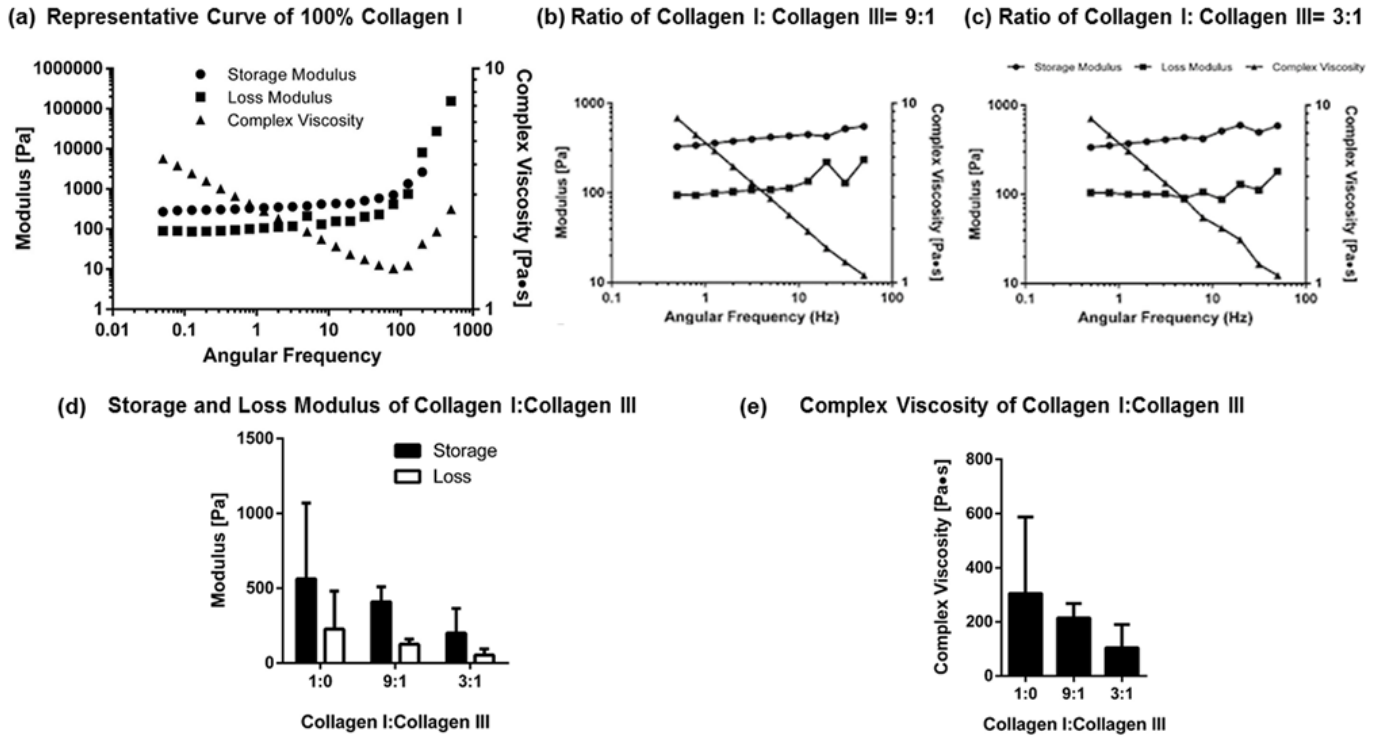

Fig. 2: Rheology analysis of Collagen gels obtained from a disc shaped (8 mm) sample. **(a)** Representative curve of frequency independent behavior of 100% Collagen I gels. A large frequency range (0.01-1000 Hz) was only performed on 100% Collagen I in order to determine how large the constant region was for the parameters studied. These results helped establish the frequency range of 0.5 to 50 Hz for testing of the Col I: III, 9:1 and 3:1 gels respectively. Equilibrium storage and loss modulus in the LVE range was found to be within 50 and 0.5 Hz for Col I: III combined in the ratios of **(b)** 9:1, and **(c)** 3:1 collagen samples.
(d) Quantification of storage and loss modulus of Collagen gels. Moduli were measured at 1.99 Hz for all samples. **(e)** Quantification of complex viscosity of Collagen gels. Viscosity was measured at 1.99 Hz for all samples.

3.3 SHG Imaging

The non-linear optical method of SHG microscopy has recently emerged as a powerful non-destructive tool for visualizing the supramolecular assembly of collagen in tissues at a great level of precision and detail (X. Chen et al. 2012). Among the collagens, Col types I and II form aligned fibers and can be detected using SHG imaging (Campagnola 2011). In contrast, collagen types III and IV are not fibrillar and therefore do not produce sufficient SHG signals for imaging (Cox et al. 2003). Based on this knowledge, we hypothesized that images acquired from gels with varying Col I:III ratios would exhibit SHG signals with changing intensity as the amount of Col I varied

proportionately in characteristic samples. Results allowed a comparison of the acquired SHG images of self-assembled proportionately in characteristic samples. Results allowed a comparison of the acquired SHG images of self-assembled collagen gels which showed a similar fiber alignment in all cases but a significantly different distribution in intensity (*$p<0.05$) as the amount of Col I decreased proportionately in gels having Col I:III of 1:0 to 9:1 and in 3:1 (Fig. 3 a-f). In Fig. 3d, e, f, SHG images of self-assembled gels from Col I:III in the ratio of 1:0 ($p=0.024$), 9:0 ($p=0.006$) and 3:1 ($p=0.001$) confirmed a similar fiber alignment in all cases yet varying image intensities in all samples (Figure 3g). The average fiber length of Col I acquired in each sample, 49 ± 6.43 μm for the 1:0, 48.63 ± 7.99 μm for the 9:1 and 48.63 ± 7.01 μm for the 3:1 respectively were not statistically different when compared across different samples (Fig. 3g).

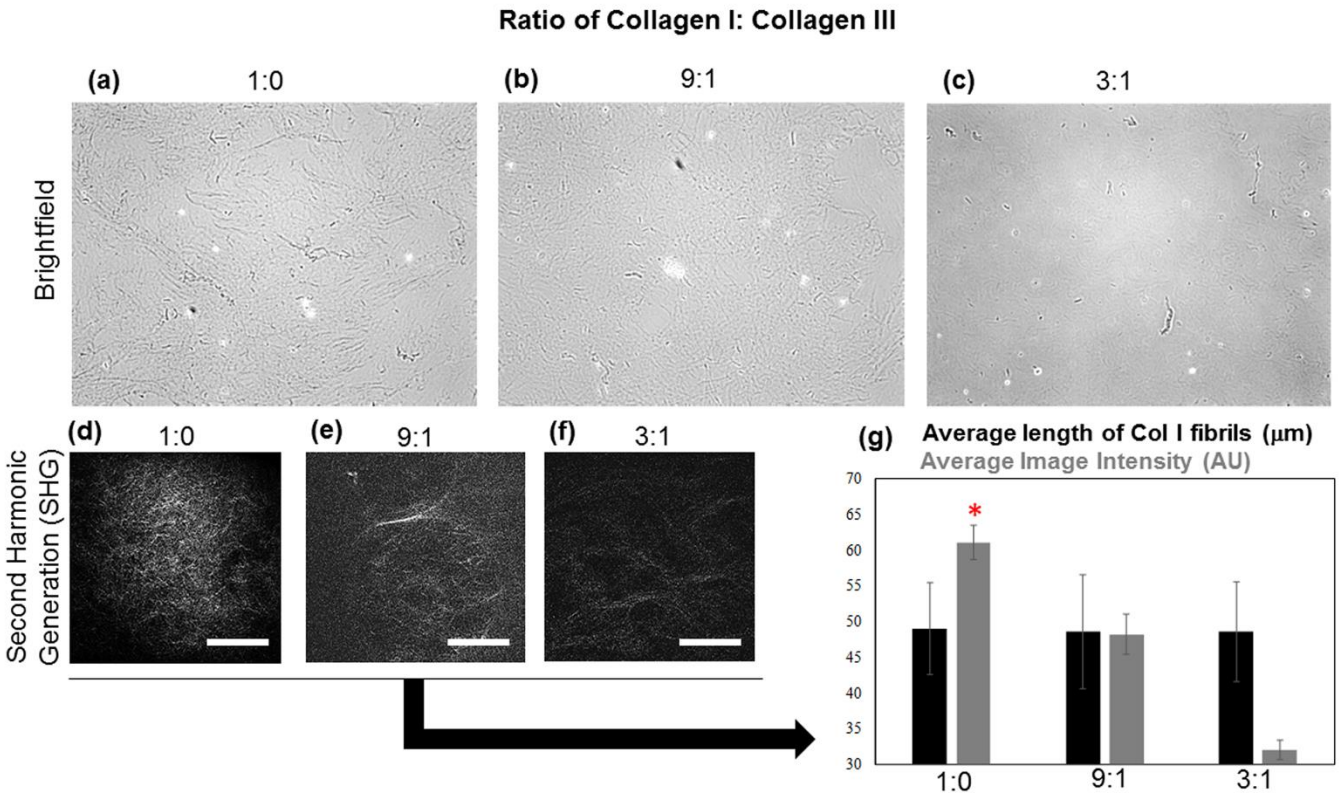

Fig. 3: Second Harmonic Generation Imaging and Analysis. Shown in **(a-c)** are representative brightfield images of the Collagen gels acquired using a 10X objective. In **(d), (e)** and **(f)** montage of SHG imaging of collagen gels are shown. Scale bar denotes 50 μm in all images.
(g) Average length ± SD of Col I for each sample is depicted (black bars) alongside average image intensity ± SD represented as a bar graphs (gray bars). Average intensity of Col I fibers significantly reduced in samples with proportionate increase of Col III. * indicates statistically significant data with $p<0.05$.

These results confirmed the identify and constitution of the varying ratios of the Col I:III in the assembled gels. Comparative images acquired using brightfield imaging also qualitatively confirmed the same (Fig. 3a-c). Our SHG images were comparable to images of other self-assembled collagen gels reported in published studies (X. Chen et al. 2012). Phenol Red solution used as a control for this experiment provided a signal in the green channel, but not in the blue channel, indicating the presence of Phenol Red and its lack of SHG signals (Supplementary Figure 3).

3.4 Structural Analysis

Cross-sectional SEM images of gels with varying Col I:III revealed varying structural characteristics among the different gels, where the 3:1 ratio was observed to be highly organized and striated with homogeneous distribution of pores (Fig. 4c), while 1:0 and 9:1 lacked fibril organization associated with non-homogenously distributed pores (Fig. 4a, b). This difference in structural composition led to varying average pore diameters across each collagen ratio, with 1:0, 9:1 and 3:1 having an average pore diameter of 16.33±6.23 μm, 14.65±6.06 μm, and 13.83±7.54 μm respectively (Fig. 4d), although the values were not significantly different. There is an accumulation of fibers at higher concentrations of Col I, which leave greater gaps in the scaffold structure (Asgari et al. 2017).

3.5 Cell Proliferation

CM proliferation was estimated through flow cytometry (FACS) following pre-staining by Cell Trace Violet (CTV) with fluorescence dimming with each new generation of CM. After a 24hr period, 97.95%, 94.12%, and 95.05% CM that expressed the CTV dye were detected in the samples prepared from the 1:0, 9:1, and 3:1 gels respectively (Fig.5 a–c) with the positive control expressing 98.58% CTV-stained CM. On the contrary the negative controls expressed only a negligible amount of 4.85%. After 72 hrs, 65.17%, 81.73%, and 89.44% of CTV-stained CM were detected in the samples prepared from the 1:0, 9:1, and 3:1 gels respectively. The extent of cell proliferation within the 1:0, 9:1, and 3:1 gels was calculated to be 8.6%, 12.6% and 30.5% for each of

these gels respectively, as shown on Figure 5d. The presence of multiple peaks is representative of successive generations of CM (Fig.5 a–c) (Anil Kumar et al. 2018; Severin and Ohnemus 1982). CM proliferation was seen to increase with the decrease of Col I, pointing to reduced cell division within the fibrous habitat of post-infarction myocardial tissue (Tseliou et al. 2014).

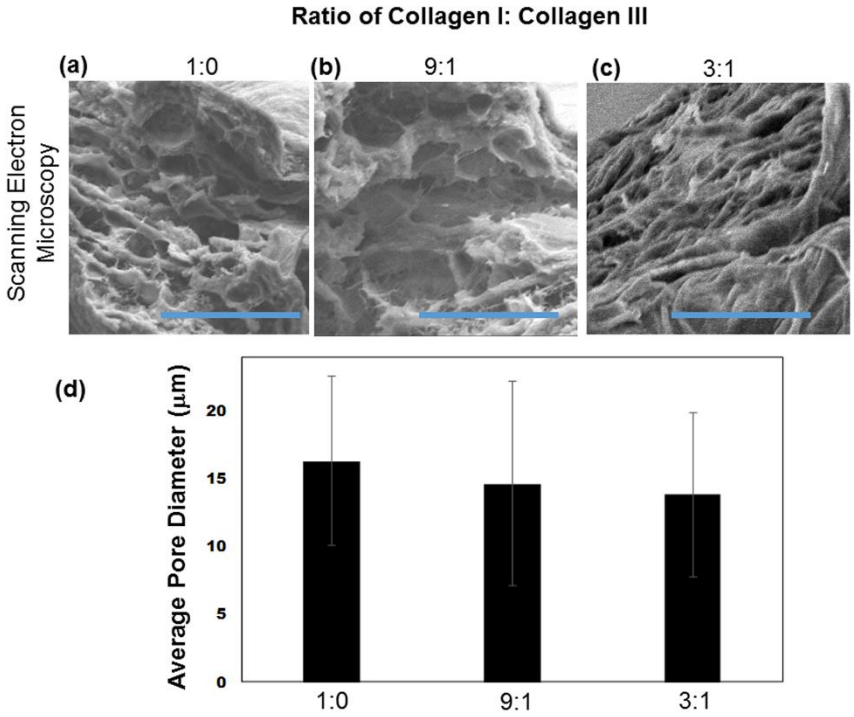

Fig. 4: Scanning Electron Microscopy (SEM) Imaging and Analysis. Shown in (a-c) are representative SEM images of the porosity of Collagen gels. Cross-sectional view of gels containing (a) 100% Collagen I, (b) Collagen I:III=9:1 and (c) Collagen I:III=3:1. Scale bar denotes 50 µm in all images.
(d) Average ± SD of pore diameter for each gel represented as a bar graph.

3.6 Resultant Cell Morphology and Force Estimation

The resultant morphology of the CM varied based on the characteristic gel, the cells were cultured. CM in Col I:III, 1:0 and 9:1 gels were shown to exhibit a change in morphology as they transformed from their normal rod-shape to a shorter morphology as seen in Figure 6a and b. In contrast, CM in 3:1 gels maintained their elongated rod-shaped morphology (Fig. 6c). CM were found to have proliferated in all samples, hence images were obtained from areas of relatively lower cell density to capture the characteristic morphology of each case. Cells cultured within 1:0 gels had an average length of 63.16±10.36 µm and measured 63.89±9.85 µm on 9:1 gels while those on 3:1 gels distinctively measured 86.01±28.83 µm (*$p<0.05$ compared to other cases) maintaining a

length closest to the known 100 µm end-to-end length for in vivo CM (Göktepe et al. 2010) (Fig. 6d). The relationship established between the average end-to-end length of CM and the Young's modulus of each gel substrate is depicted in Figure 6d, where cell length was seen to decrease with the proportional increase in the substrate stiffness varied by the amount of Col I incorporated. Average cell diameter was also seen to vary across

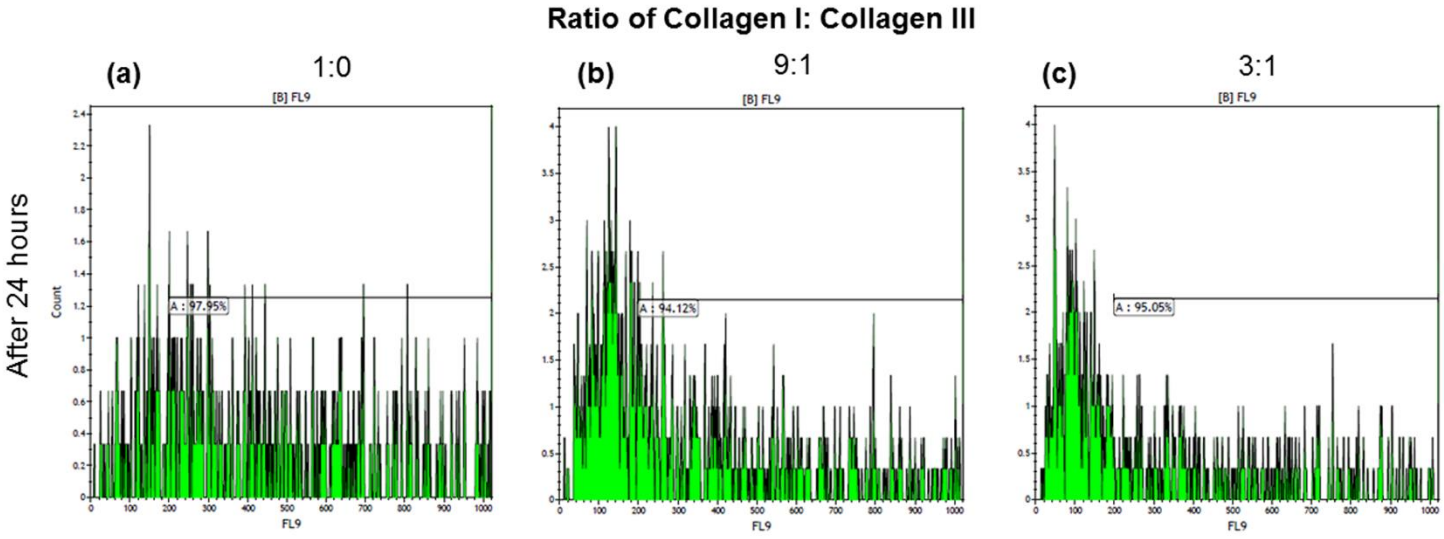

(d)

Collagen I: III	After 24 hours	After 72 hours	Extent of proliferation (%)
1:0	97.95	89.44	8.6
9:1	94.12	81.73	12.6
3:1	95.05	65.17	30.5
Positive Control	98.58	No Significant Change	
Negative Control	4.85	No Significant Change	

Fig. 5: Human cardiomyocytes cultured in Collagen gels and analyzed for Cell Trace Violet (CTV) expression through Flow Cytometry (FACS) analysis. Trends of cell proliferation are shown for gels with Collagen I: Collagen III at **(a)** 1:0, **(b)** 9:1, and **(c)** 3:1 ratios after 24 hr of culture.
(d) Shown are the % of cells expressing the CTV dye, obtained from different samples at respective time points. Samples included the Collagen gels and Controls. Positive Controls included cells that were treated with the CTV and Negative Controls included cells cultured without the addition of the CTV dye. Extent of proliferation was obtained by identifying the difference between both incubation periods for each respective ratio and normalizing the result over the 24 hr. time point for 1:0 or gels with a 100% Collagen I. The extent of proliferation was shown to increase with the decrease of Collagen I, indicating cardiomyocyte proliferation under a less-stiffer or compliant environment.

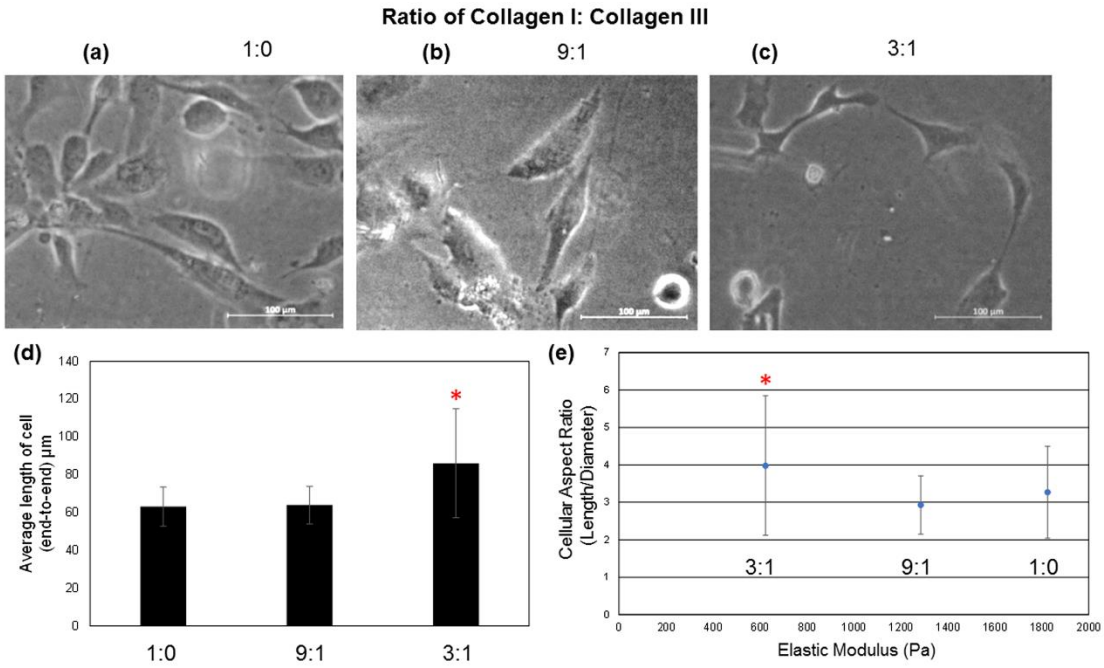

Fig. 6: Comparison of Cell Morphologies for Human AC16 Cardiomyocytes grown atop gels containing Collagen I:Collagen III as **(a)** 1:0, **(b)** 9:1, and **(c)** 3:1 after 48 hr of in vitro culture. Average end-to-end length of the cells was measured **(d)** for each case and the data represented as bar graphs show the Average Length ± SD of cells in each gel. Cells exhibited a characteristic rod like shape with the decrease of Collagen I content in the gels, indicating a healthy and functional cardiomyocyte morphology. * indicates statistically significant data with $p<0.05$. **(e)** Cellular Aspect Ratio vs Elastic Modulus of Collagen gels. Increase in the aspect ratio was evidenced with a decrease in the amount of Collagen I, and proportionate increase of Collagen III.

samples with measurements of 20.5±4.23 µm, 22.52±3.7 µm, and 23.59±6.91 µm for Col I:III in ratios of 1:0, 9:1, and 3:1 respectively. Thus, cell morphology and parameters were altered due to a change in the Young's modulus, as a rise in the amount of Col I leads to an increase in CM diameter and a shorter end-to-end average cell length. This led to varying cellular aspect ratios for the 1:0, 9:1, and 3:1 cases, with values of 3.3±1.2, 2.9±0.8, and 4.0±1.9 being calculated respectively (Fig. 6e). A higher Young's modulus, characteristic of a stiffer environment within the cardiac muscle, can therefore be attributed to the subsequent Col I build up following fibrosis bringing about a loss of contractility (Harvey and Leinwand 2011; Richardson et al. 2015; Talman and Ruskoaho 2016; Lindsey et al. 2015). The resulting loss in the contractile ability of the cardiac tissue in such circumstances could be a possible outcome of decreased end-to-end cell lengths imparting a rounded morphology

to the CM, in contrast to their elongated nature, which is characteristic of healthy CM. This may lead to decoupling of the electrically conductive CM with their counterparts (Kohl and Gourdie 2014). Controls as shown in Supplementary Fig. 4, depicted a normal elongated cell morphology when cultured atop plastic tissue culture wells. Cell force analysis revealed applied stress to be centralized for cells cultured within Col I:III gels in the ratio of 1:0 and 9:1 (Fig. 7a, b), but equally dispersed for 3:1 samples (Fig. 7c). For the 1:0 and the 9:1 gels, resultant tensile forces within the cells showed an unequal distribution of forces with an increase of maximum stress applied towards the center (Fig. 7a, b).

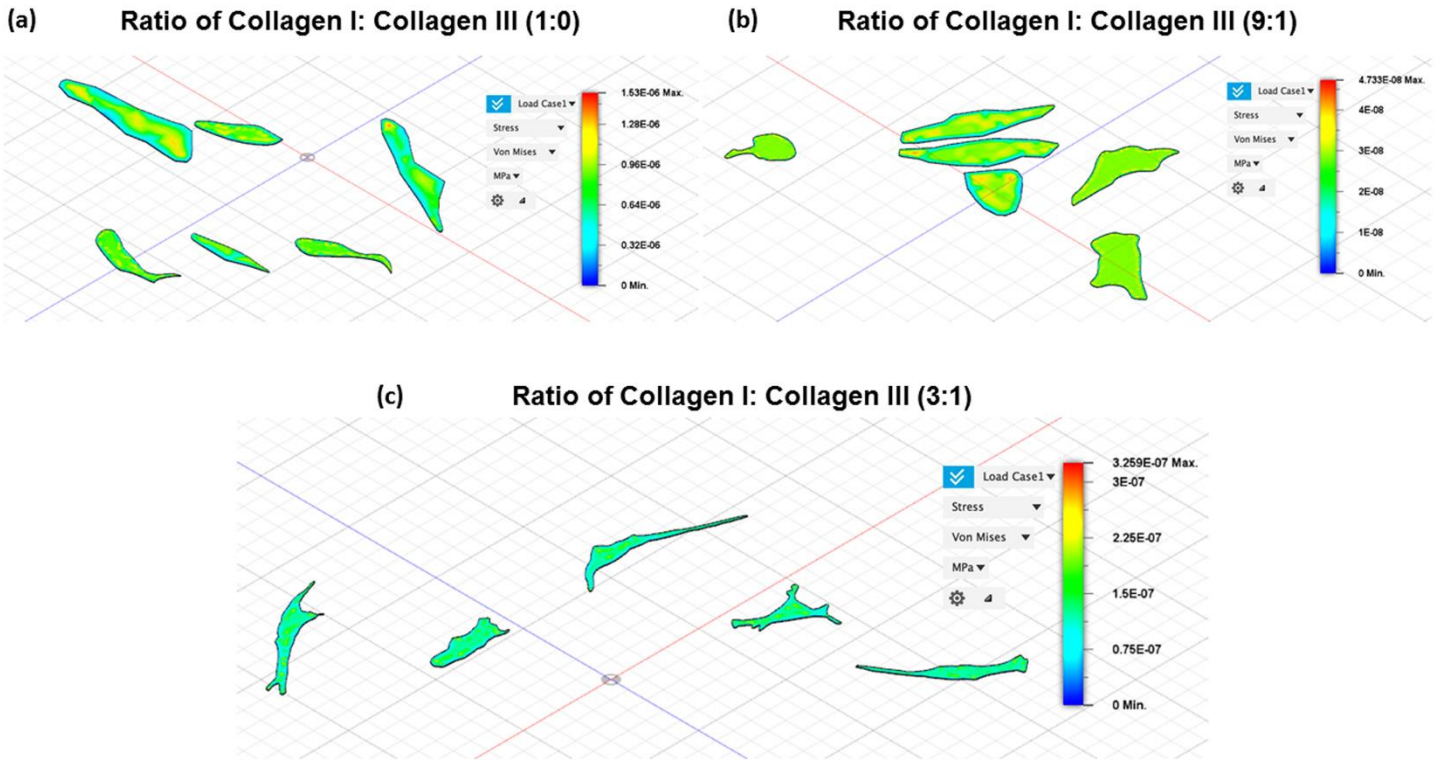

Fig. 7: Cell force analysis of cardiomyocytes atop Col I:III ratio **(a)**1:0, **(b)** 9:1, and **(c)**3:1. Maximum stress is seen to be applied to cells cultured in the 1:0 and the 9:1 gels, but not the 3:1 gels where the forces on the cells appear homogenously distributed.

The increase of central tensile forces in cells in the 9:1 gels is similar to the 1:0 ratio, where the lack of cellular elements of compression caused an increase of traction forces onto the gel's surface (Ingber 2003). An overall less elongated cell morphology in Col I:III, 1:0 and 9:1 samples can be attributed to a disruption of the

regular alignment of microtubules within the cells' cytoskeleton. Due to the absence of this element, traction forces applied by cells onto the gels' surface increases, as microtubules have been found to sustain compression forces within the cell, stabilizing both cell shape and cell-surface tensile forces (Ingber 2003). Tensile forces within cells cultured in 3:1 gels were found to be well distributed, in contrast (Fig. 7c). Conserved cell morphology of CM allows for an element of compression within the cytoskeleton of the cells, preventing them from exhibiting traction forces upon the surface of the collagen gel in accordance with the tensegrity model (Ingber 2003). A clear distinction was seen in cells cultured atop 3:1 gels compared to other cases, with normal cell morphology being conserved, as the presence of aligned microtubules provides an element of compression, which counteracts tension forces intrinsic to the cytoskeleton of cells.

4. Discussion

This study incorporated combinations of Col I and III within a gel scaffold to bring about an understanding of fibrillogenesis within the heart as a result of an unbalance in homeostatic Col I and III concentrations. Confirmation of gelation was hence required, with an absorbance assay to demonstrate fibril formation over time for the Col I:III gels containing 9:1 and 3:1 ratios of Col I and III respectively. A reduction in transmittance indicated the formation of fibrils and an increase in their density, as less light was allowed to penetrate through the solidifying opaque gels. Over a 5-minute time frame, 9:1 and 3:1 Col I:III gels demonstrated a drop in transmittance presenting evidence of conclusion of the process of gelation. The curves were similar to that found in previous work, with collagen gels undergoing turbidity assays measuring absorbance, a measurement whose relationship with transmittance is defined as $A = log\left(\frac{1}{T}\right)$ in accordance with the Beer-Lambert Law (Li et al. 2009; Lewis 2016).

Characterization of 1:0, 9:1, and 3:1 gel samples through rheology was performed to estimate the average Young's modulus and complex viscosity, and hence understand how increased concentrations of Col I can impact CM. A significant reduction in the mechanical properties of these gels with the decrease in proportion of Col I

was observed. Subsequent deposition of thicker Col I fibers on the infarcted cardiac tissue, corresponding to the 9:1 gel sample, may thus cause it to stiffen and lose its contractile ability resulting in cardiac arrests over time.

In this study, for the very first time SHG imaging was used to detect and confirm collagen fibril formation in self-assembled gels using varying ratios of Col I:III, and distinguish between these gels based on the results obtained. The primary advantage of SHG over other imaging techniques is the ability to directly visualize protein assemblies without relying on inferences from using of exogenous labels, and further, to extract more structural information via polarization and directional resolved methods (Lacomb et al. 2009). Furthermore, this technique is non-destructive and will be of added advantage when these unique compositions of Col I:III are adopted towards 3D printing of Collagen based scaffolds for tissue engineering.

For each gel ratio in question, a relationship between average pore diameter and Col I concentration was established, with the pore diameter of each sample increasing along with their respective Col I composition. Such connections can be attributed to the density of the fibers, which are, as demonstrated by rheology, of wider range in samples of greater Col I ratio. This increase of fiber diameter results in a smaller number of fibers required to achieve a stabilized gel structure, generating a greater amount of spacing between fibers, and consequently, an increased porosity (Asgari 2017).

The CTV assay suggested greater cell proliferation in a 3:1 environment as compared to those of 9:1 and 1:0 of Col I:III. Such implication is justified, as a 3:1 ratio of Col I:III is found in healthy cardiac tissue, while overproduction of collagen in the 9:1 case, is characteristic of cardiac muscle tissue post myocardial infarction (Jugdutt 2003; Pauschinger et al. 1998). This finding illustrates the impact fibrillogenesis has on the heart, with CM being placed under strain as the surrounding ECM becomes increasingly fibrous (Pandey et al. 2018).

Cell morphology studied following the culture of cells in each collagen gel, revealed a change in shape, which may indirectly correlate with the acute damage to CM brought about by a myocardial infarction. Typical CM structure can be described as a long, rectangular rod, which allows for the smooth contraction of the myocardium (Jian et al. 2016). In contrast, fibrotic myocardium contains round and condensed CM that increase the difficulty of cardiac contraction (Guo et al. 2018). This alteration of morphology after a myocardial infarction complicates

contraction of the heart and facilitates the occurrence of relapsing episodes, as a fibrotic left ventricle becomes a weak spot that is unable to withstand the same load as previously capable.

Shear forces applied by CM onto their respective collagen ratios, indicated traction forces involving 1:0 and 9:1 samples were focused towards the center, while those in 3:1 were equally distributed within each cell. The assertive distinction between shear forces can be attributed to the tensegrity model discussed by Ingber et al., in which he states cell geometry of unhealthy cells sees a decrease in microtubules throughout the cytoskeleton (Ingber 2003). Such macrofilaments are responsible for sustaining compression throughout the cell, balancing internal tension throughout the cell and allowing for healthy cell morphology. Balanced internal forces within cells then prevent traction forces from being applied onto the culturing surface, allowing for a homogenous distribution of shear stress.

5. Conclusion

A newly developed collagen gel system composed of Col I and III was engineered to mimic conditions of the cardiac muscle characteristic of a healthy and a diseased state. Physical properties of each collagen gel sample were analyzed with the purpose of understanding how variation of Col I quantities alter gel morphology. Along with these morphological changes, CM shape was assessed for each collagen I:III ratio to establish knowledge of the geometric reaction CM undergo when exposed to post-myocardial infarction conditions, with respect to a Col I rich ECM. Cellular force analysis was a necessary technique that illustrated the resultant stress on the CM within the collagen gel samples in question in a quantitative manner. Overall, our results demonstrate the effects of increased amounts of Col I on CM and their ECM, highlighting the importance of studying the physiological changes of the heart after a myocardial infarction, as this change in ECM and cell morphology facilitates reoccurrences and leads to lasting complications. By applying tools of engineering to create such a usable biological model, this study will ultimately, lead to the development of a validated living model of a healthy cardiac tissue unit that can support improved fundamental understanding of pathological conditions. This model is versatile and can be adopted by others working with cell types including epithelial or endothelial cells, to

understand their cross talk and role in complex tissue behavior, such as in lung- (Gabasa et al. 2017) and vascular-fibrosis (Huveneers, Daemen, and Hordijk 2015).

ACKNOWLEDGMENT

The Joddar Lab (IMSTEL) acknowledges NIH BUILD Pilot 8UL1GM118970-02, NIH 1SC2HL134642-01 and the NSF-PREM program (DMR 1205302). CQ Li acknowledges the NSF MRI grant #DBI 1429708. The authors acknowledge, with pleasure, support from the National Science Foundation with NSF-PREM grant #DMR-1827745, and the NSF-MRI grant # DMR-1828268. This manuscript is a contribution from Center for Advanced Materials Research (CMR), established at UTEP with the funding received from the National Science Foundation. We also acknowledge the technical assistance received from Dr. Armando Varela for kindly assisting us with the bright field microscopy and Dr. David Roberson for his help with the SEM.

References

1. Acosta, Yassel, Qi Zhang, Arifur Rahaman, Hugues Ouellet, Chuan Xiao, Jianjun Sun, and Chunqiang Li. 2014. “Imaging Cytosolic Translocation of Mycobacteria with Two-Photon Fluorescence Resonance Energy Transfer Microscopy.” *Biomedical Optics Express* 5 (11): 3990. https://doi.org/10.1364/boe.5.003990.
2. Anil Kumar, Shweta, Shane C. Allen, Nishat Tasnim, Tahmina Akter, Shinhye Park, Alok Kumar, Munmun Chattopadhyay, Yoshihiro Ito, Laura J. Suggs, and Binata Joddar. 2019. “The Applicability of Furfuryl-Gelatin as a Novel Bioink for Tissue Engineering Applications.” *Journal of Biomedical Materials Research - Part B Applied Biomaterials* 107 (2): 314–23. https://doi.org/10.1002/jbm.b.34123.
3. Asgari, Meisam, Neda Latifi, Hossein K. Heris, Hojatollah Vali, and Luc Mongeau. 2017. “In Vitro Fibrillogenesis of Tropocollagen Type III in Collagen Type i Affects Its Relative Fibrillar Topology and Mechanics.” *Scientific Reports*. https://doi.org/10.1038/s41598-017-01476-y.
4. Blissett, Angela R., Derek Garbellini, Edward P. Calomeni, Cosmin Mihai, Terry S. Elton, and Gunjan

Agarwal. 2009. "Regulation Of Collagen Fibrillogenesis By Cell Surface Expression Of Kinase Dead DDR2. "*Journal of Molecular Biology* 385 (3): 902–11. https://doi.org/10.1016/j.cgh.2008.07.016.Cytokeratin.

5. Brower, Gregory L., Jason D. Gardner, Mary F. Forman, David B. Murray, Tetyana Voloshenyuk, Scott P. Levick, and Joseph S. Janicki. 2006. "The Relationship between Myocardial Extracellular Matrix Remodeling and Ventricular Function." *European Journal of Cardio-Thoracic Surgery* 30 (4): 604–10. https://doi.org/10.1016/j.ejcts.2006.07.006.
6. Campagnola, Paul. 2011. "Second Harmonic Generation Imaging Microscopy: Applications to Diseases Diagnostics." *Analytical Chemistry* 83 (9): 3224–31. https://doi.org/10.1021/ac1032325.
7. Carrow, James K., Punyavee Kerativitayanan, Manish K. Jaiswal, Giriraj Lokhande, and Akhilesh K. Gaharwar. 2015. "Polymers for Bioprinting." In *Essentials of 3D Biofabrication and Translation*. https://doi.org/10.1016/B978-0-12-800972-7.00013-X.
8. Chang, Fred, and Kerwyn C. Huang. 2014. "How and Why Cells Grow as Rods." *BMC Biology*. https://doi.org/10.1186/s12915-014-0054-8.
9. Chen, Xiyi, Oleg Nadiarynkh, Sergey Plotnikov, and Paul J Campagnola. 2012. "Second Harmonic Generation Microscopy for Quantitative Analysis of Collagen Fibrillar Structure." *Nature Protocols* 7 (4): 654–69. https://doi.org/10.1038/nprot.2012.009.
10. Chen, Zhiyong, X. C.May Lu, Deborah A. Shear, Jitendra R. Dave, Angela R. Davis, Clifford A. Evangelista, Danelle Duffy, and Frank C. Tortella. 2011. "Synergism of Human Amnion-Derived Multipotent Progenitor (AMP) Cells and a Collagen Scaffold in Promoting Brain Wound Recovery: Pre-Clinical Studies in an Experimental Model of Penetrating Ballistic-like Brain Injury." *Brain Research* 1368: 71–81. https://doi.org/10.1016/j.brainres.2010.10.028.
11. Chistiakov, Dimitry A., Alexander N. Orekhov, and Yuri V. Bobryshev. 2016. "The Role of Cardiac Fibroblasts in Post-Myocardial Heart Tissue Repair." *Experimental and Molecular Pathology*. Academic

Press Inc. https://doi.org/10.1016/j.yexmp.2016.09.002.

12. Cox, Guy, Eleanor Kable, Allan Jones, Ian Fraser, Frank Manconi, and Mark D. Gorrell. 2003. "3-Dimensional Imaging of Collagen Using Second Harmonic Generation." *Journal of Structural Biology* 141 (1): 53–62. https://doi.org/10.1016/S1047-8477(02)00576-2.
13. Fan, Dong, Abhijit Takawale, Jiwon Lee, and Zamaneh Kassiri. 2012. "Cardiac Fibroblasts, Fibrosis and Extracellular Matrix Remodeling in Heart Disease." *Fibrogenesis and Tissue Repair*. https://doi.org/10.1186/1755-1536-5-15.
14. Frahs, Stephanie M., Julia Thom Oxford, Erica E. Neumann, Raquel J. Brown, Cynthia R. Keller-Peck, Xinzhu Pu, and Trevor J. Lujan. 2018. "Extracellular Matrix Expression and Production in Fibroblast-Collagen Gels: Towards an In Vitro Model for Ligament Wound Healing." *Annals of Biomedical Engineering*, 2018. https://doi.org/10.1007/s10439-018-2064-0.
15. Frisk, Michael, Marianne Ruud, Emil K.S. Espe, Jan Magnus Aronsen, Åsmund T. Røe, Lili Zhang, Per Andreas Norseng, et al. 2016. "Elevated Ventricular Wall Stress Disrupts Cardiomyocyte T-Tubule Structure and Calcium Homeostasis." *Cardiovascular Research* 112 (1): 443–51. https://doi.org/10.1093/cvr/cvw111.
16. Gabasa, Marta, Paula Duch, Ignasi Jorba, Alícia Giménez, Roberto Lugo, Irina Pavelescu, Fernando Rodríguez-Pascual, et al. 2017. "Epithelial Contribution to the Profibrotic Stiff Microenvironment and Myofibroblast Population in Lung Fibrosis." *Molecular Biology of the Cell* 28 (26): 3741–55. https://doi.org/10.1091/mbc.e17-01-0026.
17. Glowacki, Julie, and Shuichi Mizuno. 2008. "Collagen Scaffolds for Tissue Engineering." *Biopolymers*. https://doi.org/10.1002/bip.20871.
18. Göktepe, Serdar, Oscar John Abilez, Kevin Kit Parker, and Ellen Kuhl. 2010. "A Multiscale Model for Eccentric and Concentric Cardiac Growth through Sarcomerogenesis." *Journal of Theoretical Biology*. https://doi.org/10.1016/j.jtbi.2010.04.023.
19. Guo, Guang Ran, Liang Chen, Man Rao, Kai Chen, Jiang Ping Song, and Sheng Shou Hu. 2018. "A

Modified Method for Isolation of Human Cardiomyocytes to Model Cardiac Diseases." *Journal of Translational Medicine* 16 (1). https://doi.org/10.1186/s12967-018-1649-6.

20. Huveneers, Stephan, Mat J.A.P. Daemen, and Peter L. Hordijk. 2015. "Between Rho(k) and a Hard Place." *Circulation Research* 116 (5): 895–908. https://doi.org/10.1161/circresaha.116.305720.
21. Ingber, D. E. 2003. "Tensegrity I. Cell Structure and Hierarchical Systems Biology." *Journal of Cell Science* 116 (7): 1157–73. https://doi.org/10.1242/jcs.00359.
22. Jian, Zhong, Yi Je Chen, Rafael Shimkunas, Yuwen Jian, Mark Jaradeh, Karen Chavez, Nipavan Chiamvimonvat, et al. 2016. "In Vivo Cannulation Methods for Cardiomyocytes Isolation from Heart Disease Models." *PLoS ONE* 11 (8). https://doi.org/10.1371/journal.pone.3474065.
23. Joddar, Binata, Eduardo Garcia, Atzimba Casas, and Calvin M. Stewart. 2016. "Development of Functionalized Multi-Walled Carbon-Nanotube-Based Alginate Hydrogels for Enabling Biomimetic Technologies." *Scientific Reports* 6 (August). https://doi.org/10.1038/srep32456.
24. Jugdutt, Bodh I. 2003. "Ventricular Remodeling after Infarction and the Extracellular Collagen Matrix: When Is Enough Enough?" *Circulation*. https://doi.org/10.1161/01.CIR.0000085658.98621.49.
25. Kohl, Peter, and Robert G. Gourdie. 2014. "Fibroblast-Myocyte Electrotonic Coupling: Does It Occur in Native Cardiac Tissue?" *Journal of Molecular and Cellular Cardiology* 70: 37–46. https://doi.org/10.1016/j.yjmcc.2013.12.024.
26. Lacomb, Ronald, Oleg Nadiarnykh, Sallie S Townsend, and Paul J Campagnola. 2009. "Phase Matching Considerations in Second Harmonic Generation from Tissues: Effects on Emission Directionality, Conversion Efficiency and Observed Morphology" 281 (7): 1823–32.
27. Lewis, Peter Rhys. 2016. "Sample Examination and Analysis." In *Forensic Polymer Engineering*, 33–69. Elsevier. https://doi.org/10.1016/b978-0-08-101055-6.00002-1.
28. Li, Yuping, Amran Asadi, Margo R. Monroe, and Elliot P. Douglas. 2009. "PH Effects on Collagen Fibrillogenesis in Vitro: Electrostatic Interactions and Phosphate Binding." *Materials Science and*

Engineering C 29 (5): 1643–49. https://doi.org/10.1016/j.msec.2009.01.001.

29. Nielsen, M.J., and M. A. Karsdal. 2016. *Type III Collagen*. *Biochemistry of Collagens, Laminins and Elastin: Structure, Function and Biomarkers*. Elsevier Inc. https://doi.org/10.1016/B978-0-12-809847-9.00002-7.
30. Pandey, Pragati, William Hawkes, Junquiang Hu, William Valentine Megone, Julien Gautrot, Narayana Anilkumar, Min Zhang, et al. 2018. "Cardiomyocytes Sense Matrix Rigidity through a Combination of Muscle and Non-Muscle Myosin Contractions." *Developmental Cell* 44 (3): 326-336.e3. https://doi.org/10.1016/j.devcel.2017.12.024.
31. Pathak, Manas, Sagartirtha Sarkar, Elangovan Vellaichamy, and Subha Sen. 2001. "Role of Myocytes in Myocardial Collagen Production." *Hypertension* 37 (3): 833–40. https://doi.org/10.1161/01.HYP.37.3.833.
32. Pauschinger, Matthias, Andrea Doerner, Andrew Remppis, Roman Tannhäuser, Uwe Kühl, and Heinz Peter Schultheiss. 1998. "Differential Myocardial Abundance of Collagen Type I and Type III MRNA in Dilated Cardiomyopathy: Effects of Myocardial Inflammation." *Cardiovascular Research*. https://doi.org/10.1016/S0008-6363(97)00217-4.
33. Ribeiro, Alexandre J. S., Yen-Sin Ang, Ji-Dong Fu, Renee N. Rivas, Tamer M. A. Mohamed, Gadryn C. Higgs, Deepak Srivastava, and Beth L. Pruitt. 2015. "Contractility of Single Cardiomyocytes Differentiated from Pluripotent Stem Cells Depends on Physiological Shape and Substrate Stiffness." *Proceedings of the National Academy of Sciences*. https://doi.org/10.1073/pnas.1508073112.
34. Richardson, William J., Samantha A. Clarke, T. Alexander Quinn, and Jeffrey W. Holmes. 2015. "Physiological Implications of Myocardial Scar Structure." *Comprehensive Physiology* 5 (4): 1877–1909. https://doi.org/10.1002/cphy.c140067.
35. Severin, E., and B. Ohnemus. 1982. "Flow Cytometric Analysis of Chromosomes and Cells Using a Modified BrdU-Hoechst Method." *Histochemistry* 76 (1): 113–21. https://doi.org/10.1007/BF00493290.

36. Shayegan, Marjan, and Nancy R. Forde. 2013. "Microrheological Characterization of Collagen Systems: From Molecular Solutions to Fibrillar Gels." *PLoS ONE* 8 (8): 23–28. https://doi.org/10.1371/journal.pone.0070590.
37. Stuart, Kate, and Alyssa Panitch. 2009. "Characterization of Gels Composed of Blends of Collagen l, Collagen III, and Chondroitin Sulfate." *Biomacromolecules*. https://doi.org/10.1021/bm800888u.
38. Talman, Virpi, and Heikki Ruskoaho. 2016. "Cardiac Fibrosis in Myocardial Infarction—from Repair and Remodeling to Regeneration." *Cell and Tissue Research*. https://doi.org/10.1007/s00441-016-2431-9.
39. Tracy, Richard E. 2014. "Cardiac Myocyte Sizes in Right Compared with Left Ventricle during Overweight and Hypertension." *Journal of the American Society of Hypertension* 8 (7): 457–63. https://doi.org/10.1016/j.jash.2014.05.004.
40. Tseliou, Eleni, Geoffrey De Couto, John Terrovitis, Baiming Sun, Liu Weixin, Linda Marbán, and Eduardo Marbán. 2014. "Angiogenesis, Cardiomyocyte Proliferation and Anti-Fibrotic Effects Underlie Structural Preservation Post-Infarction by Intramyocardially-Injected Cardiospheres." *PLoS ONE* 9 (2). https://doi.org/10.1371/journal.pone.0088590.
41. Weber, Karl T., and Javier Díez. 2016. "Targeting the Cardiac Myofibroblast Secretome to Treat Myocardial Fibrosis in Heart Failure." *Circulation: Heart Failure*. https://doi.org/10.1161/CIRCHEARTFAILURE.116.003315.
42. Yu, Yuexin, Guotian Yin, Shisan Bao, and Zhikun Guo. 2018. "Kinetic Alterations of Collagen and Elastic Fibres and Their Association with Cardiac Function in Acute Myocardial Infarction." *Molecular Medicine Reports* 17 (3): 3519–26. https://doi.org/10.3892/mmr.2017.8347.